PHOTONICS Research

High efficiency generation of tunable ellipse perfect vector beams

Lin Li,[1] Chenliang Chang,[1,2,3] Caojin Yuan,[1] Shaotong Feng,[1] Shouping Nie,[1] Zhi-Cheng Ren,[2] Hui-Tian Wang,[2] and Jianping Ding[2,4]

[1]Jiangsu Key Laboratory for Opto-Electronic Technology, School of Physics and Technology, Nanjing Normal University, Nanjing 210023, China
[2]National Laboratory of Solid State Microstructures and School of Physics, Nanjing University, Nanjing 210093, China
[3]e-mail: changchenliang@njnu.edu.cn
[4]e-mail: jpding@nju.edu.cn

Received 13 June 2018; revised 1 September 2018; accepted 12 October 2018; posted 12 October 2018 (Doc. ID 335066); published 19 November 2018

We present a highly efficient method of generating and shaping ellipse perfect vector beams (EPVBs) with a prescribed ellipse intensity profile and continuously variant linear polarization state. The scheme is based on the coaxial superposition of two orthogonally polarized ellipse laser beams of controllable phase vortex serving as the base vector components. The phase-only computer-generated hologram is specifically designed by means of a modified iteration algorithm involving a complex amplitude constraint, which is able to generate an EPVB with high diffraction efficiency in the vector optical field generator. We experimentally demonstrate that the efficiency of generating the EPVB has a notable improvement from 1.83% in the conventional complex amplitude modulation based technique to 11.1% in our method. We also discuss and demonstrate the simultaneous shaping of multiple EPVBs with independent tunable ellipticity and polarization vortex in both transversal (2D) and axial (3D) focusing structures, proving potentials in a variety of polarization-mediated applications such as trapping and transportation of particles in more complex geometric circumstances.

https://doi.org/10.1364/PRJ.6.001116

1. INTRODUCTION

In recent years, the complex manipulation of amplitude, phase, and polarization of light beams has been extensively studied. People are finding new applications in the optics world that benefit from the modulation of polarization, which is an important feature of light beams. In particular, vector beams (VBs) with inhomogeneous polarization distribution, as an extension and application of conventional homogeneous polarization beams, have shown great potential in particle trapping [1], optical micromanipulation [2], high capacity information coding [3], super-resolution imaging [4], and laser processing [5]. Motivated by these applications, various methods for generating VBs have been proposed. One of them, called the static method, directly converts the homogeneous polarization state of a traditional laser mode into an inhomogeneous one by using a liquid crystal gel [6], a subwavelength metal grating [7], a rotating Glan polarizing prism [8], a spatial varying retarder [9,10], and a *Q*-plate [11,12]. On the grounds of the superposition principle with orthogonal polarization components, VBs with spatially variant polarization distribution are generated based on various types of interferometers [13–15]. Although these methods possess high diffraction efficiency, they have a common disadvantage that they lack flexibility and dynamic tunability with the special optical elements. The special fabrication techniques lead to the loss of flexibility. For the sake of flexibly controlling the polarization state of a beam, a number of approaches for generating VBs via a programmable spatial light modulator (SLM) have been presented [16–20], by virtue of the superposition principle with orthogonal polarization components. It is required to impart the desired phase to the orthogonal polarization components, which are usually implemented with the specific designed amplitude or phase type computer-generated hologram (CGH).

The cylindrical VB (CVB) is the most dramatic among the VBs due to the cylindrical symmetry in polarization distribution. Machavariani *et al.* proposed a method of creating CVB based on the axial intracavity birefringence [21]. In 2014, Yi *et al.* utilized two cascaded metasurfaces to generate cylindrical vector vortex beams, which possess both vector polarization and helical phase [22]. Then Chen *et al.* observed a novel interferometric approach to generate arbitrary CVB on the higher order Poincáre sphere [23]. Besides, femtosecond CVBs with arbitrary polarization order have also been obtained by employing half wave plates and vortex retarders [24]. However, the intensity profile of the constituent vortices generated by traditional methods is strongly dependent on their topological charges.

Subsequently, the concept of perfect VBs (PVBs) was proposed, where the beam size is independent of the polarization vortex [25]. The PVB can be produced based on a liquid crystal SLM (LC-SLM) [26] and a stable Sagnac-like interferometer [27]. Most recently, Pradhan *et al.* reported and demonstrated the generation of high-purity perfect CVBs (PCVBs) by means of an interferometric method employing an SLM. The ring diameter and ring width of the PCVB can be controlled independently [28].

However, in all the reported works that we are aware of, PVB has only a single sample mode in the record plane, namely, a bright ring curve. The circular PVB has already been studied for quite a long time, and it is not universal in some complex structured optical fields, such as asymmetric optical fields. On the other hand, beam shaping with various models in the scalar field has been extensively studied. In particular, the elliptic beams have aroused great interest due to their distinctive shape. Chakraborty and Ghosh reported a technique for the generation of elliptic hollow beams by using a scaled version of higher-order Bessel beams [29], and diffraction-free beams with an elliptic Bessel envelop were observed in periodic media [30]. In 2017, Kovalev *et al.* considered an elliptic perfect optical vortex (EPOV) and derived the exact analytical expressions for the total orbital angular momentum (OAM) and OAM density [31]. Further, EPOVs with high mode purity were obtained by freely transforming the modes of perfect optical vortices [32]. The number of optical vortices as well as the eccentricity of the elliptic trajectory can also be easily regulated by this new structure, which paves the way for new applications such as complex optical tweezers.

Meanwhile, the improvement of efficiency in generating optical vortex beams still remains challenging work. Although diffractive optical elements or CGHs are generally designed as phase-only type to achieve a higher available ratio of light, the requirement of simultaneously shaping amplitude and phase (known as complex amplitude modulation) still restricts its final efficiency, owing to the fact that the widely used complex amplitude modulation techniques are commonly based on the phase grating encoded CGH where the optical filtering configuration is necessary to select the desired complex field information [33–35]. On the other hand, an alternative method of the Gerchberg–Saxton (GS) iterative algorithm [36] and some modification versions [37] can achieve a higher diffraction efficiency for optical beam shaping, but it can only control the amplitude or phase of the generated beam, failing to regulate both.

In this paper, we extend the scalar EPOV scheme to the generation and shaping of ellipse PVBs (EPVBs). We propose a highly efficient phase-only holographic beam shaping technique capable of generating two ellipse laser beams with mutually orthogonal polarization serving as base vector components with controllable phase variation, and then collinearly superpose them to produce the EPVB. By exploiting our previously proposed vector optical field generator (VOFG) [19,20] and a newly developed phase-only CGH calculation scheme, the desired EPVB with prescribed ellipse intensity profile and continuous variant linear polarization state is experimentally generated under a significantly improved light energy efficiency of 11.1%. We also demonstrate that simultaneously generating multiple EPVBs with independent tunable ellipticity and polarization vortex is achieved in both two-dimensional (2D) and three-dimensional (3D) focal structures. Our method enriches the modes of PVBs, which could open up novel applications such as complex optical manipulation.

2. THEORY

A. Highly Efficient Phase-Only Holographic Beam Shaping

A scalar beam whose intensity and phase distribution follow a prescribed 2D curve in the focal plane of a Fourier lens can be designed based on a reported holographic beam shaping technique [38]. Briefly, the complex amplitude at the incident plane of a focusing (Fourier transform) system is written specifically as

$$H(x,y)=\int_0^T \varphi(x,y,t)\sqrt{[x_0'(t)]^2+[y_0'(t)]^2}\,\mathrm{d}t. \tag{1}$$

Here the term $\varphi(x,y,t)$ shapes the phase of the beam along the desired curve represented by $c_2(t)=(x_0(t),y_0(t))$ in the Cartesian coordinate with $t\in[0,2\pi]$ and is expressed by

$$\varphi(x,y,t)=\exp\left\{\frac{i}{\omega_0^2}[yx_0(t)-xy_0(t)]+\frac{i\sigma}{\omega_0^2}\int_0^\tau[x_0(\tau)y_0'(\tau)-y_0(\tau)x_0'(\tau)]\mathrm{d}\tau\right\}, \tag{2}$$

where w_0 is a constant, $x_0'(t)=\mathrm{d}x_0(t)/\mathrm{d}t$, and $y_0'(t)=\mathrm{d}y_0(t)/\mathrm{d}t$. σ is a free parameter that allows varying the phase gradient along the curve if needed and is also independent from the size of the beam.

Equation (1) is used to generate a structurally stable scalar focal beam, whose intensity distribution and phase gradient are specially designed. First of all, we consider the generation of a 2D elliptic curve of $x_0(t)=a\cdot R\cdot\cos t$, $y_0(t)=b\cdot R\cdot\sin t$, where $t\in[0,2\pi]$. The parameters a and b are the positive constant and act as the scaling factor to realize the mode conversion from ring to ellipse. The modes and ellipticity of the EPVB can be modulated arbitrarily by adjusting the scaling factors a and b while the topological charge of the phase vortex along the ellipse curve is well defined by the parameter σ. As an illustration, Fig. 1 shows the simulated results of two shaped ellipse beams under the same dimension ($R=0.15$ mm, $a=1$, $b=0.75$) but different phase gradients (i.e., topological charge $l_1=2$ and $l_2=4$) by the Fourier transform of the calculated incident field $H(x,y)$. Figures 1(a) and 1(c) display the intensity distributions of the resulting beams while Figs. 1(b) and 1(d) are the corresponding phase distributions. Note that the

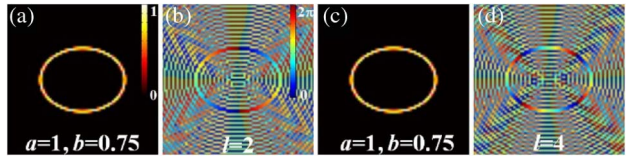

Fig. 1. Reconstructed results of the ellipse beams with different topological charges [$l_1=2$ for (a) and (b), $l_2=4$ for (c) and (d)]. (a) and (c) are the intensity distributions. (b) and (d) are the phase distributions with differently marked topological charges.

dimensions of the two generated ellipse beams are independent of the different topological charges. This is pivotal to guarantee the yield of the ellipse "perfect" VB in the following descriptive orthogonal superposition procedure.

In order to create the EPVB, we use the aforementioned technique to shape the two spatially superposed scalar ellipse curves, which have a mutually orthogonal polarization state, and combine the VOFG [19,20] to create the desired structures of the EPVB. The complex amplitude fields at the incident plane, denoted as $H_L(x,y)$ and $H_R(x,y)$, are separately calculated by using Eq. (1), and they are responsible for generating two base elliptic scalar beams in the focal volume. The scheme of VOFG is separating the desired pair of base component beams [H_L (x, y) and H_R (x, y)] into two optical channels via imposing respective phase shifting factors of $\exp(i2\pi x \sin\theta_x/\lambda)$ and $\exp(i2\pi y \sin\theta_y/\lambda)$ and converting them into a mutually orthogonal polarization state by using two wave plates [quarter-wave plates (QWPs) or half-wave plates]. The fast-axis orientations of the two employed wave plates are perpendicular to each other. Therefore, when the two separated base beams $H_L(x,y)$ and $H_R(x,y)$ pass through each wave plate exclusively, they can convert to mutually orthogonal circular or linear polarization states. Thus, the total complex amplitude hologram at the incident plane of the VOFG system is calculated by

$$E_{\text{total}}(x,y) = H_L(x,y)\cdot\exp(i2\pi x \sin\theta_x/\lambda) + H_R(x,y)\cdot\exp(i2\pi y \sin\theta_y/\lambda). \quad (3)$$

Since $E_{\text{total}}(x,y)$ calculated by Eq. (3) is a complex value that is composed of amplitude and phase components, we wish to use a phase-only CGH $\exp[i\varphi(x,y)]$ to represent this complex hologram $E_{\text{total}}(x,y) = A_{\text{total}}(x,y)\exp[i\varphi_{\text{total}}(x,y)]$ because of the employed phase-only SLM in the optical experiment. A famous method to obtain the phase-only CGH is by means of encoding the amplitude $A_{\text{total}}(x,y)$ and phase $\varphi_{\text{total}}(x,y)$ into a phase-only holographic grating, in which the phase factor $\varphi(x,y)$ is calculated as [39,40]

$$\varphi(x,y) = A_{\text{total}}(x,y)\varphi_{\text{total}}(x,y). \quad (4)$$

In this way, the complex amplitude $E_{\text{total}}(x,y) = A_{\text{total}}(x,y)\exp[i\varphi_{\text{total}}(x,y)]$ can be recovered from the first diffraction order of the encoded phase-only CGH $\exp[i\varphi(x,y)]$. The spatial filtering that is performed with the $4f$ optical system permits selecting the corresponding desired terms. However, this widely used encoding technique suffers from a problem of relatively low light efficiency when generating the desired VBs, owing to the existence of unnecessary diffraction orders in the filtering plane as shown in Fig. 2(a). The dotted lines indicate the desired first order information which will be allowed to pass the filter at the Fourier plane. An impressive amount of energy is wasted due to the block of useless orders.

In order to improve the diffraction efficiency and avoid the energy loss, we propose an alternative phase-only CGH encoding method, where the unnecessary diffraction orders can be eliminated in order to notably improve the light energy efficiency. This method is inspired and modified from the previously reported double constraint GS (DCGS) algorithm [41,42] in order to create a phase-only incident pattern $\exp[i\varphi(x,y)]$ to control the particular focal complex amplitude. Briefly, assuming that

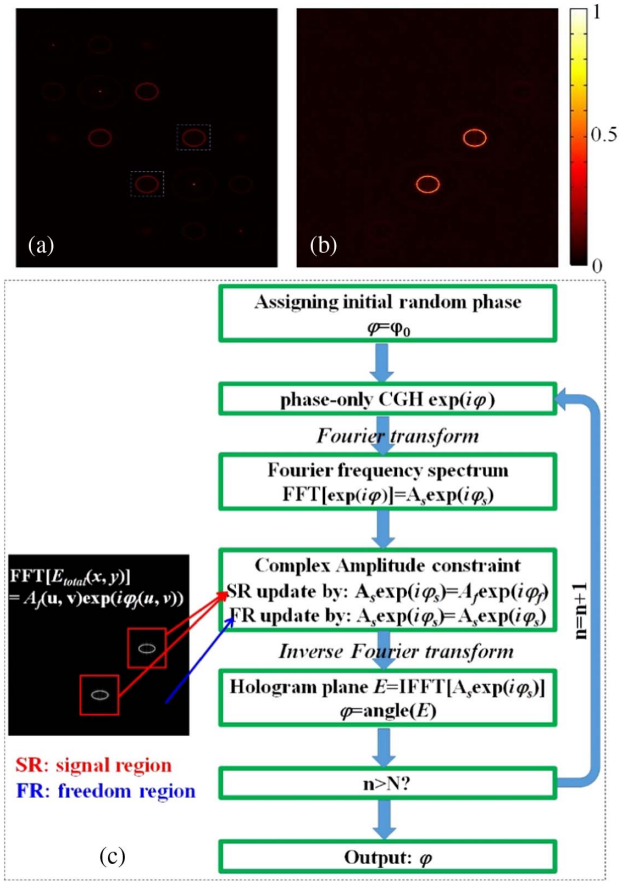

Fig. 2. Intensity distributions at the filtering (Fourier) plane from the phase-only CGH calculated by (a) the grating encoding method and (b) the proposed F-DCGS method. (c) Flow chart of the proposed F-DCGS algorithm.

the focal plane of the incident complex amplitude $E_{\text{total}}(x,y)$ is calculated by its Fourier transform as $\text{FT}[E_{\text{total}}(x,y)] = A_f(u,v)\exp[i\varphi_f(u,v)]$, we aim to calculate a functionally equivalent phase-only CGH $\exp[i\varphi(x,y)]$ that also satisfied the relations by $\text{FT}\{\exp[i\varphi(x,y)]\} = \text{FT}[E_{\text{total}}(x,y)] = A_f(u,v)\cdot\exp[i\varphi_f(u,v)]$, in such a way that the phase wavefront $\exp[i\varphi(x,y)]$ can be considered as a highly approximate substitute of the complex wavefront $E_{\text{total}}(x,y)$ to guarantee the accurate complex amplitude shaping in the Fourier frequency domain. As a result, the issue is converted into a well-known phase retrieval case where we need to obtain the phase $\varphi(x,y)$ from its complex amplitude Fourier spectrum $A_f(u,v)\exp[i\varphi_f(u,v)]$, which can be solved by using the proposed iteration framework, named as the frequency-domain DCGS (F-DCGS) algorithm.

The flow chart of the proposed F-DCGS routine to calculate the phase-only $\varphi(x,y)$ is plotted in Fig. 2(c). We first set the random phase distribution $\varphi_0(x,y)$ as an initial guess; then it is Fourier transformed to the frequency spectrum domain (Fourier domain) by using the numerical fast Fourier transform (FFT) algorithm. In the Fourier domain, there are two allocated regions, denoted as signal region (SR) and freedom region (FR). The SR contains the beams (i.e., the ellipse beams) where the target complex amplitude $A_f(u,v)\exp[i\varphi_f(u,v)]$ is used to

replace the calculated one, while in the FR (almost the zero intensity background) there is no constraint applied and just the calculated complex amplitude $A_s(u,v)\exp[i\varphi_s(u,v)]$ remains. The updated complex field in the frequency domain is then propagated backward to the incident hologram plane by inverse-FFT (IFFT) operation. The amplitude of the calculated hologram is constrained and set as a uniform distribution, whereas the phase is preserved. The process continues until a predefined maximum iteration number N is reached and the phase component of the hologram is extracted as a phase-only output of the F-DCGS algorithm.

The main metric of the F-DCGS method is the high diffraction efficiency in recovery of arbitrary desired complex amplitude at the Fourier plane from the phase-only CGH. For a better view we also show the plots of the reconstructed intensity at the Fourier plane in Fig. 2(b). Compared with Fig. 2(a), the redundant diffraction components are obviously suppressed except for some faint background noise, indicating that almost all the light energy is diffracted to the desired beams, thus achieving a high efficiency VOFG system enabled by F-DCGS-based phase-only CGH.

B. Optical Setup for Generating a High Efficiency EPVB

The optical experiment of generating an EPVB is based on our previously reported VOFG system [19,20]. The benefits of VOFG include great flexibility and convenient adjustment in terms of the control over the space variant beam amplitude, phase, and state of polarization compared with other existing schemes. As is sketched in Fig. 3, a fundamental Gaussian beam from a solid-state laser with a wavelength of 532 nm is expanded and collimated by sequentially passing through two convex lenses before they interact with the phase-only CGH digitally imprinted on the SLM (Holoeye Leto, 6.4 μm pixel pitch, 1920 × 1080 resolution). The diffracted beams from the reflective SLM travel through a $4f$ optical filtering configuration so that they project to the back aperture of the Fourier transform lens (L_3, $f = 100$ mm). Due to the function of the imposed offset phase term, the diffraction light reflected from the SLM is spatially filtered toward different directions—the horizontal and vertical directions. Two QWPs placed at the filtering plane play a role to convert the separated beams into left and right circular polarization components, which serve as a pair of base beams for the subsequent vectorial superposition.

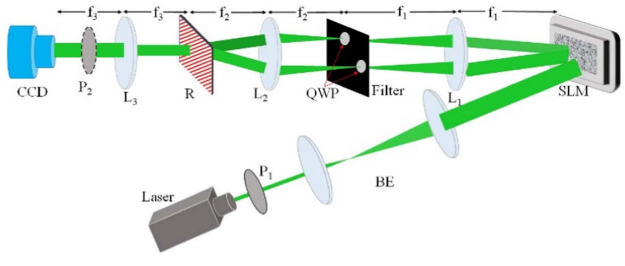

Fig. 3. Schematic representation of the experiment setup for generating an EPVB. P, polarizer; BE, beam expander; SLM, spatial light modulator; L, convex lenses ($f_1 = 400$ mm, $f_2 = 300$ mm, and $f_3 = 100$ mm); QWP, quarter-wave plate; R, Ronchi grating; CCD, charge-coupled device.

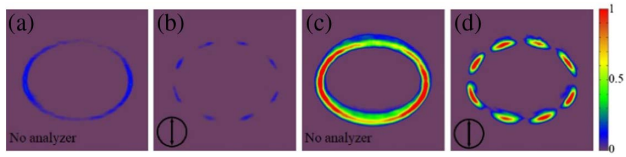

Fig. 4. Generated intensity of the EPVB from the phase-only CGH calculated (a), (b) by the grating encoding method and (c), (d) by the F-DCGS method. The arrow marks in (b) and (d) indicate the polarization direction of an analyzer before the CCD.

A Ronchi grating is also appended at the output plane of the $4f$ configuration to enable the recollinear propagation of the two base vector beams. The angle between the grid lines of the Ronchi grating and the horizontal direction (x-axis) is adjusted to 45°. The Fourier lens L_3 is used to transform the field distribution of the laser beam so as to generate the EPVB in the focal region. Finally, the charge coupled device (CCD) camera captures the intensity profile of the generated EPVB.

We compare the efficiency of generating the EPVB from two phase-only CGHs that are calculated by using our proposed F-DCGS algorithm and the conventional grating encoding method of Eq. (4), respectively. The two orthogonal base ellipse beams are calculated under the same dimensions ($R = 0.15$ mm, $a = 1$, $b = 0.75$) but different topological charges of $l_1 = 4$ and $l_2 = -4$, so the generated vector ellipse has a varied linear polarization state along the curved path. Displayed in Figs. 4(a) and 4(b) are the experimental intensity from the grating encoded phase-only CGH (the case of polarizer angle marks in the lower left corner). Figures 4(c) and 4(d) are the corresponding results from the proposed F-DCGS based phase-only CGH, showcasing distinct high beam intensity and the successful enhancing of the light diffraction efficiency in our VOFG system. The quantitative measured diffraction efficiency is 5.53 μW/302.6 μW = 1.83% for Fig. 4(a) and 33.62 μW/302.6 μW = 11.1% for Fig. 4(c), by separately placing an optical power meter on the CCD plane and before the SLM.

3. EXPERIMENT RESULTS

The first experiment is to generate a single EPVB in the focal region. It is synthesized from two base vector complex amplitude ellipses. We adjust the topological charges (l_1, l_2) of the two ellipses to control the polarization vortex distribution along the curve and use a polarization analyzer (linear polarizer P_2) to observe the intensity variation induced by the specific polarization distribution of the generated EPVB. The polarization vortex composed of continuous variation of the linear polarization state obeys the formula of $N = |l_2 - l_1|$. The intensity distributions of the EPVB with different polarization vortices are experimentally measured at the focal plane by the CCD, as illustrated in Fig. 5. Figures 5(a)–5(e) are the generated EPVB with different scaling factors of ($a = 1$, $b = 0.5$), ($a = 1$, $b = 0.75$), ($a = 1$, $b = 1$), ($a = 0.75$, $b = 1$), and ($a = 0.5$, $b = 1$). The first column shows the intensity patterns of different ellipticity when no analyzer is used, while the results from the second to seventh columns are the experimental intensity

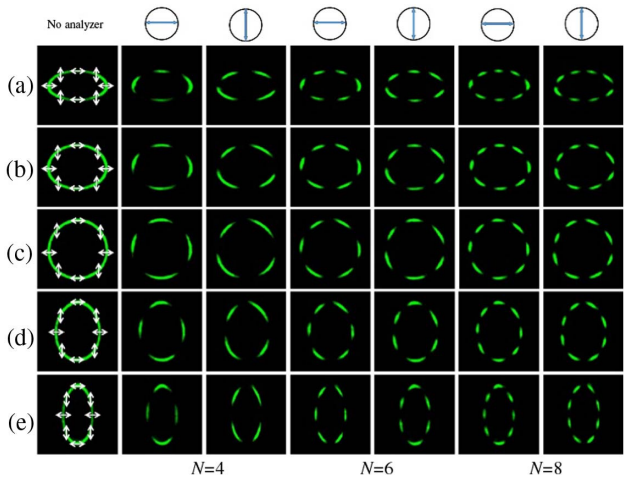

Fig. 5. Experimental results of generating EPVBs under different ellipse modes and topological charges. The scaling factors are (a) $a = 1$, $b = 0.5$; (b) $a = 1$, $b = 0.75$; (c) $a = 1$, $b = 1$; (d) $a = 0.75$, $b = 1$; (e) $a = 0.5$, $b = 1$.

distributions at the CCD plane under different polarization vortices (the number of intensity extinction in each mode) of $N = 4$, 6, and 8, when an analyzer is inserted by rotating its angle to 0° or 90°. Figure 5(c) represents a ring shape ($a = 1$, $b = 1$) that corresponds to the well-known PCVB mode, and it is obvious that the EPVB can be easily transformed from circle to ellipse by adjusting the scaling factors, as depicted in other results.

Next, we demonstrate the simultaneous generation of multiple EPVBs consisting of various spatial modes from a single phase-only CGH. First of all, each incident complex field hologram in charge of shaping each individual EPVB is calculated by Eq. (3), and then all the obtained holograms are multiplexed into a final hybrid complex incident hologram after multiplying a separately assigned shifting phase factor (also called the carrier wave). The expression of the final complex hologram shaping the number of n EPVBs takes the final form

$$E_{\text{hybrid}}(x,y) = \sum_{i=1}^{n} E_{\text{total-}i}(x,y) \cdot \exp\left[ik\left(\frac{xu_i}{f} + \frac{yv_i}{f}\right)\right], \quad \textbf{(5)}$$

where $E_{\text{total-}i}(x,y)$ represents the ith hologram to generate the ith EPVB mode, which is calculated from Eq. (3). f is the focal length of the Fourier transform lens. The wave number k obeys the expression of $k = 2\pi/\lambda$. The frequency coordinates (u_i, v_i) determine the transversal displacement of each generated EPVB in the focal plane. The final complex hologram $E_{\text{hybrid}}(x,y)$ is encoded into phase-only CGH by using the proposed F-DCGS method as mentioned in Section 2.A. Figure 6 illustrates the experimental intensity distribution of simultaneous generation of four EPVB modes (1: $a = 1$, $b = 0.5$; 2: $a = 0.5$, $b = 1$; 3: $a = 1$, $b = 0.75$; 4: $a = 0.75$, $b = 1$) under two analyzer directions. The polarization vortex of each mode from location serial number (1)–(4) is $N = 4$, $N = 6$, $N = 8$, and $N = 10$, respectively. The pattern extinction phenomenon appears in each mode, and the extinction numbers are different from each other determined by the topological charges of the orthogonal

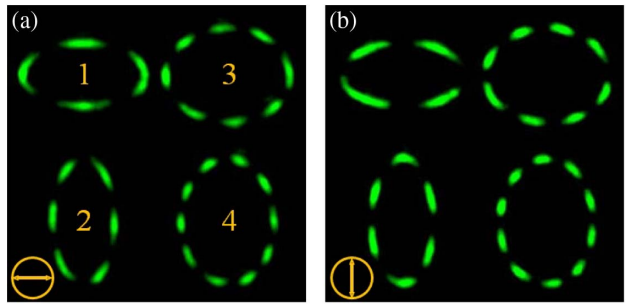

Fig. 6. Experimental intensity profiles of generating hybrid EPVBs after two analyzer directions.

ellipse beams. It should be mentioned that although we only demonstrated the generation of four EPVBs here, the proposed scheme also allows for the multiplex of more beams in various modes simultaneously [43].

Second, we exhibit a small expansion to another type of asymmetric vector beams, namely, rectangle PVBs (RPVBs). In the same way as calculating the elliptic curve, we apply the scaling factors a and b to control the length–width ratio in the parametric expressions of the 2D rectangle curve as $x_0(t) = a \cdot R \cdot [-2\cos(t) + 0.3\cos(3t)]$, $y_0(t) = b \cdot R \cdot [-2\sin(t) - 0.3\sin(3t)]$, where $t \in [0, 2\pi]$ and $R = 0.15$ mm. Figures 7(a)–7(d) show the experimental results of four generated RPVBs under different scaling factors of ($a = 1$, $b = 0.5$), ($a = 1$, $b = 0.75$), ($a = 0.75$, $b = 1$), and ($a = 0.5$, $b = 1$), respectively. The first column shows the measured total intensity patterns of the RPVB when no analyzer is used, while the second and third columns correspond to the experimental intensity distributions when an analyzer is rotated to 0° and 90°, respectively. The number of intensity extinctions in each mode is $N = 8$. We also experimentally demonstrate the simultaneous generation of multiple RPVBs containing four different modes (1: $a = 1$, $b = 0.5$; 2: $a = 0.5$, $b = 1$; 3: $a = 1$, $b = 0.75$; 4: $a = 0.75$, $b = 1$), as shown in Figs. 7(e) and 7(f).

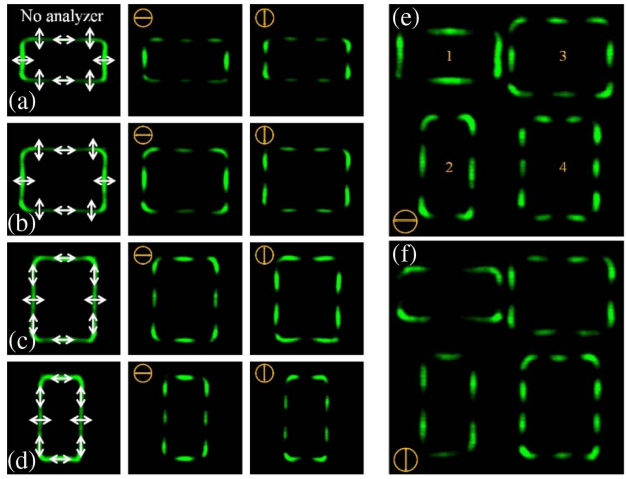

Fig. 7. Experimental intensity patterns of the generated RPVBs. (a)–(d): RPVBs under different scaling modes of ($a = 1$, $b = 0.5$), ($a = 1$, $b = 0.75$), ($a = 0.75$, $b = 1$), and ($a = 0.5$, $b = 1$). (e) and (f) show hybrid RPVBs after two analyzer directions.

The extinction phenomenon is observed in each mode under two analyzer directions, and the polarization vortices in each mode are $N = 4$, 6, 8, and 10, respectively.

A significant feature of the proposed high efficiency EPVB shaping technique is the high axial intensity gradient under the focusing, which is increasingly desirable in the field of optical trapping and manipulation, for example, in the transfer of orbital angular momentum from light to microparticles [1,2]. Meanwhile, it is common knowledge that each orthogonal component of the ellipse perfect vortex curve can also be realized by modulating an ellipse Bessel beam [30–32], where the generation of such a kind of beam has diffraction-free performance through axial propagation and does not have a high axial intensity gradient. The simulations of diffraction effects for one base (scalar) ellipse perfect vortex ($R = 0.15$ mm, $a = 1$, $b = 0.5$, $l = 4$) in the focal region are carried out as observed in Fig. 8. We calculate the propagation of the generated curve beams along the optical axis (z direction) by using the angular spectrum diffraction algorithm [44] in a range of [−1 cm, 1 cm] from the focal plane ($z = 0$). The propagation of the beam generated by using the ellipse Bessel function method [30–32] for the xz and yz planes, displayed in Fig. 8(a), shows a low axial intensity gradient from the shape-invariant phenomenon except for a size scaling. In contrast, the counterpart by using our method shown in Fig. 8(b) confirms the generated beams have a tighter intensity profile with a high transversal intensity gradient, and this property can provide an additional degree of freedom for shaping multiple EPVBs in three dimensions. Figure 8(c) further plots the one-dimensional (x-directional) intensity profile at the $z = 0$ plane, indicating that the ellipse Bessel function method has a Gaussian intensity profile (red color line), whereas our method has a tighter intensity profile (blue color line).

Based on the high intensity gradient of a single EPVB, we finally consider the generation of multiple EPVBs in different focusing planes. By introducing an extra axially shifting phase, each mode of the EPVB is axially relocated to a required target plane away from the customary focal plane of the Fourier transform lens, enabling simultaneously reconstructing all the EPVBs in multiple planes. For the sake of three-dimensionally shifting each mode to its own target position, the phase term imposed on each complex incident field hologram $E_{\text{total}-i}(x, y)$ is represented by

$$\phi_i(x, y) = kz_i\sqrt{1 - \frac{x^2}{f^2} - \frac{y^2}{f^2}} + k\left(\frac{xu_i}{f} + \frac{yv_i}{f}\right), \tag{6}$$

where z_i is the distance from the ith EPVB mode to the focal plane and f is the focal length of the Fourier lens (L_3 in Fig. 3). Note that the function of the quadratic phase term in Eq. (6) axially shifts the ith EPVB mode to its desired depth. The final complex hologram $E_{3D}(x, y)$ at the incident field for simultaneously shaping multiple EPVBs is calculated by coherent complex superposition of all the single holograms as

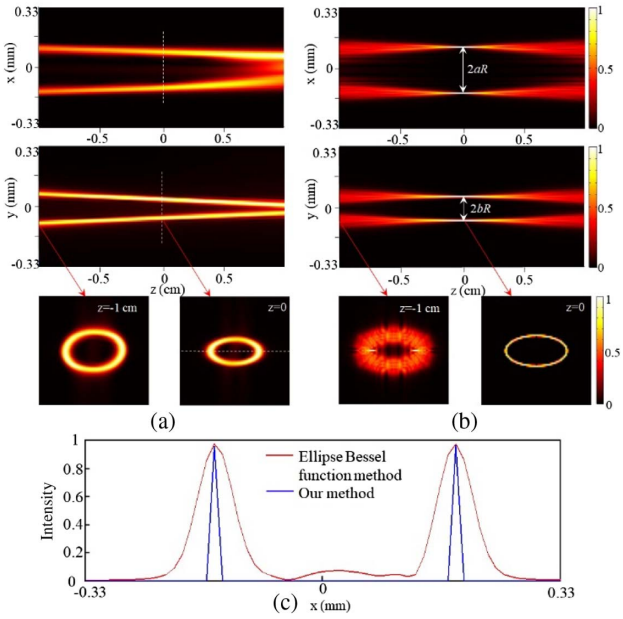

Fig. 8. Beam propagation in the xz and yz planes are displayed for the case of two beam shaping techniques. (a) Ellipse Bessel function method [30–32]. (b) Our method. The beam intensity profiles before ($z = -1$ cm) and at ($z = 0$) the focal plane are also shown in each case. (c) The one-dimensional beam intensity profile of the two methods at $z = 0$ (red and blue color lines, respectively).

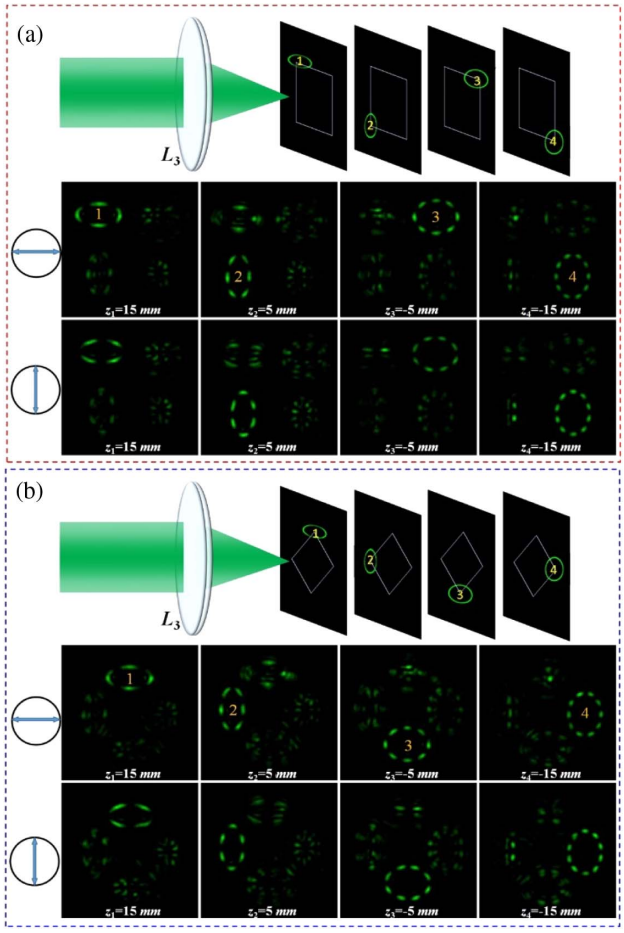

Fig. 9. Experimental results of the generated hybrid EPVBs in two different types of three-dimensional layouts under different analyzer directions.

$$E_{3D}(x,y) = \sum_{i=1}^{n} E_{\text{total}-i}(x,y) \cdot \exp[i\varphi_i(x,y)]. \quad (7)$$

Accordingly, by encoding $E_{3D}(x,y)$ into a phase-only CGH using the F-DCGS algorithm, we are able to generate multiple EPVBs where each EPVB with individually tunable ellipticity and polarization vortex is controlled to different axial and lateral locations aligned in the range of the focal regions, shaping into a multidepth 3D pattern structure.

Figure 9 shows the experimental reconstruction results consisting of four different EPVB modes at different depth planes. The focal length of L_3 is 100 mm. The four EPVBs have four different ellipticities (1: $a = 1$, $b = 0.5$; 2: $a = 0.5$, $b = 1$; 3: $a = 1$, $b = 0.75$; 4: $a = 0.75$, $b = 1$) and polarization vortices ($N = 4$, 6, 8, and 10), and they are transversally aligned along two structure types including rectangular [see Fig. 9(a)] and diamond [see Fig. 9(b)] trajectories. Meanwhile, the displacement of each EPVB to the focal plane is set by $z_1 = 15$ mm, $z_2 = 5$ mm, $z_3 = -5$ mm, and $z_4 = -15$ mm, respectively, and is recorded by moving the CCD back and forth along the z direction. The angles of the analyzer are marked on the left side of each row. It can be seen that each single EPVB is focused at the given depth plane when the rest of the EPVBs become blurred, proving the successful generation of multiple tunable EPVBs in more complex 3D geometry circumstances.

4. CONCLUSION

In summary, we present a highly efficient and flexible approach to generating arbitrary transforms of the EPVB mode by coaxial superimposition of two base ellipse perfect optical vortices. The optical experimental results verify the performance of the proposed method for shaping different modes of the EPVB in the focal plane as well as simultaneously generating multiple EPVB modes in different hybrid layouts. The proposed method of generating an EPVB has a higher diffraction conversion efficiency of up to 11.1%, which is a significant improvement compared to conventional vector beam generating systems. We expect that the proposed technique may provide more versatile vector optical field shaping in latent applications such as complex optical trapping.

Funding. National Key R&D Program of China (2018YFA0306200); National Natural Science Foundation of China (NSFC) (91750202, 11474156, 61605080, 61775097); China Postdoctoral Science Foundation (2016M601775).

REFERENCES

1. S. Roy, K. Ushakova, Q. van den Berg, S. F. Pereira, and H. P. Urbach, "Radially polarized light for detection and nanolocalization of dielectric particles on a planar substrate," Phys. Rev. Lett. **114**, 103903 (2015).
2. Y. Kozawa and S. Sato, "Optical trapping of micrometer-sized dielectric particles by cylindrical vector beams," Opt. Express **18**, 10828–10833 (2010).
3. X. P. Li, Y. Y. Cao, and M. Gu, "Superresolution-focal-volume induced 3.0 Tbytes/disk capacity by focusing a radially polarized beam," Opt. Lett. **36**, 2510–2512 (2011).
4. W. Yu, Z. Ji, D. Dong, X. Yang, Y. Xiao, Q. Gong, P. Xi, and K. Shi, "Super-resolution deep imaging with hollow Bessel beam STED microscopy," Laser Photon. Rev. **10**, 147–152 (2015).
5. R. Drevinskas, J. Zhang, M. Beresna, M. Gecevičius, A. G. Kazanskii, and Y. P. Svirko, "Laser material processing with tightly focused cylindrical vector beams," Appl. Phys. Lett. **108**, 221107 (2016).
6. H. W. Ren, Y. H. Lin, and S. T. Wu, "Linear to axial or radial polarization conversion using a liquid crystal gel," Appl. Phys. Lett. **89**, 051114 (2006).
7. W. B. Chen, W. Han, D. C. Abeysinghe, R. L. Nelson, and Q. Zhan, "Generating cylindrical vector beams with subwavelength concentric metallic gratings fabricated on optical fibers," J. Opt. **13**, 015003 (2011).
8. Q. Hu, Z. H. Tan, X. Y. Weng, H. M. Guo, Y. Wang, and S. L. Zhuang, "Design of cylindrical vector beams based on the rotating Glan polarizing prism," Opt. Express **21**, 7343–7353 (2013).
9. W. J. Lai, B. C. Lim, P. B. Phua, K. S. Tiaw, H. H. Teo, and M. H. Hong, "Generation of radially polarized beam with a segmented spiral varying retarder," Opt. Express **16**, 15694–15699 (2008).
10. Z. Liu, Y. Liu, Y. Ke, Y. Liu, W. Shu, H. Luo, and S. Wen, "Generation of arbitrary vector vortex beams on hybrid-order Poincaré sphere," Photon. Res. **5**, 15–21 (2017).
11. P. Chen, W. Ji, B. Y. Wei, W. Hu, V. Chigrinov, and Y.-Q. Lu, "Generation of arbitrary vector beams with liquid crystal polarization converters and vector-photoaligned q-plates," Appl. Phys. Lett. **107**, 241102 (2015).
12. M. M. Sánchez-López, J. A. Davis, N. Hashimoto, I. Moreno, E. Hurtado, K. Badham, A. Tanabe, and S. W. Delaney, "Performance of a q-plate tunable retarder in reflection for the switchable generation of both first- and second-order vector beams," Opt. Lett. **41**, 13–16 (2016).
13. S. C. Tidwell, D. H. Ford, and W. D. Kimura, "Generating radially polarized beams interferometrically," Appl. Opt. **29**, 2234–2239 (1990).
14. S. Liu, P. Li, T. Peng, and J. Zhao, "Generation of arbitrary spatially variant polarization beams with a trapezoid Sagnac interferometer," Opt. Express **20**, 21715–21721 (2012).
15. C. Y. Han, R. S. Chang, and H. F. Chen, "Solid-state interferometry of a pentaprism for generating cylindrical vector beam," Opt. Rev. **20**, 189–192 (2013).
16. D. Xu, B. Gu, G. Rui, Q. Zhan, and Y. Cui, "Generation of arbitrary vector fields based on a pair of orthogonal elliptically polarized base vectors," Opt. Express **24**, 4177–4186 (2016).
17. I. Moreno, J. A. Davis, T. M. Hernandez, D. M. Cottrell, and D. Sand, "Complete polarization control of light from a liquid crystal spatial light modulator," Opt. Express **20**, 364–376 (2012).
18. C. Rosales-Guzmán, N. Bhebheand, and A. Forbes, "Simultaneous generation of multiple vector beams on a single SLM," Opt. Express **25**, 25697–25706 (2017).
19. X. L. Wang, J. Ding, W. J. Ni, C. S. Guo, and H. T. Wang, "Generation of arbitrary vector beams with a spatial light modulator and a common path interferometric arrangement," Opt. Lett. **32**, 3549–3551 (2007).
20. Z. Chen, T. Zeng, B. Qian, and J. Ding, "Complete shaping of optical vector beams," Opt. Express **23**, 17701–17710 (2015).
21. G. Machavariani, Y. Lumer, I. Moshe, A. Meir, S. Jackel, and N. Davidson, "Birefringence-induced bifocusing for selection of radially or azimuthally polarized laser modes," Appl. Opt. **46**, 3304–3310 (2007).
22. X. N. Yi, X. H. Ling, Z. Y. Zhang, Y. Li, X. X. Zhou, Y. C. Liu, S. Z. Chen, H. L. Luo, and S. C. Wen, "Generation of cylindrical vector vortex beams by two cascaded metasurfaces," Opt. Express **22**, 17207–17215 (2014).
23. S. Z. Chen, X. X. Zhou, Y. H. Liu, X. H. Ling, H. L. Luo, and S. C. Wen, "Generation of arbitrary cylindrical vector beams on the higher order Poincaré sphere," Opt. Lett. **39**, 5274–5276 (2014).
24. Y. Q. Zhang, X. J. Dou, Y. Yang, C. Xie, J. Bu, C. J. Min, and X. C. Yuan, "Flexible generation of femtosecond cylindrical vector beams," Chin. Opt. Lett. **15**, 030007 (2017).
25. P. Li, Y. Zhang, S. Liu, C. Ma, L. Han, H. Cheng, and J. Zhao, "Generation of perfect vectorial vortex beams," Opt. Lett. **41**, 2205–2208 (2016).
26. S. Fu, T. Wang, and C. Gao, "Generating perfect polarization vortices through encoding liquid-crystal display devices," Appl. Opt. **55**, 6501–6505 (2016).
27. T. Wang, S. Fu, F. He, and C. Gao, "Generation of perfect polarization vortices using combined gratings in a single spatial light modulator," Appl. Opt. **56**, 7567–7571 (2017).

28. P. Pradhan, M. Sharma, and B. Ung, "Generation of perfect cylindrical vector beams with complete control over the ring width and ring diameter," IEEE Photon. J. **10**, 6500310 (2018).
29. R. Chakraborty and A. Ghosh, "Generation of an elliptic Bessel beam," Opt. Lett. **31**, 38–40 (2006).
30. J. J. Miret and C. J. Zapata-Rodríguez, "Diffraction-free beams with elliptic Bessel envelope in periodic media," J. Opt. Soc. Am. B **25**, 1–6 (2008).
31. A. A. Kovalev, V. V. Kotlyar, and A. P. Porfirev, "A highly efficient element for generating elliptic perfect optical vortices," Appl. Phys. Lett. **110**, 261102 (2017).
32. X. Z. Li, H. X. Ma, C. L. Yin, J. Tang, H. H. Li, M. M. Tang, J. G. Wang, Y. P. Tai, X. F. Li, and Y. S. Wang, "Controllable mode transformation in perfect optical vortices," Opt. Express **26**, 651–662 (2018).
33. J. A. Davis, D. M. Cottrell, J. Campos, M. J. Yzuel, and I. Moreno, "Encoding amplitude information onto phase-only filters," Appl. Opt. **38**, 5004–5013 (1999).
34. V. Arrizón, "Complex modulation with a twisted-nematic liquid-crystal spatial light modulator: double-pixel approach," Opt. Lett. **28**, 1359–1361 (2003).
35. Y. Qi, C. Chang, and J. Xia, "Speckleless holographic display by complex modulation based on double-phase method," Opt. Express **24**, 30368–30378 (2016).
36. R. W. Gerchberg and W. O. Saxton, "A practical algorithm for the determination of phase from image and diffraction plane pictures," Optik (Stuttgart) **35**, 237–246 (1972).
37. J. S. Liu and M. R. Taghizadeh, "Iterative algorithm for the design of diffractive phase elements for laser beam shaping," Opt. Lett. **27**, 1463–1465 (2002).
38. J. A. Rodrigo, T. Alieva, E. Abramochkin, and I. Castro, "Shaping of light beams along curves in three dimensions," Opt. Express **21**, 20544–20555 (2013).
39. V. Arrizón, U. Ruiz, R. Carrada, and L. A. González, "Pixelated phase computer holograms for the accurate encoding of scalar complex fields," J. Opt. Soc. Am. A **24**, 3500–3507 (2007).
40. J. A. Rodrigo, T. Alieva, A. Cámara, O. Martínez-Matos, P. Cheben, and M. L. Calvo, "Characterization of holographically generated beams via phase retrieval based on Wigner distribution projections," Opt. Express **19**, 6064–6077 (2011).
41. S. H. Tao and W. X. Yu, "Beam shaping of complex amplitude with separate constraints on the output beam," Opt. Express **23**, 1052–1062 (2015).
42. C. Chang, J. Xia, L. Yang, W. Lei, Z. Yang, and J. Chen, "Speckle-suppressed phase-only holographic three-dimensional display based on double-constraint Gerchberg–Saxton algorithm," Appl. Opt. **54**, 6994–7001 (2015).
43. C. Rosales-Guzmán, N. Bhebhe, N. Mahonisi, and A. Forbes, "Multiplexing 200 modes on a single digital hologram," J. Opt. **19**, 113501 (2017).
44. C. Schulze, D. Flamm, M. Duparré, and A. Forbes, "Beam-quality measurements using a spatial light modulator," Opt. Lett. **37**, 4687–4689 (2012).